Electronic Supplementary Material (ESI) for Journal of Materials Chemistry C.

Supporting Information

Achieving Diversified Emissive Behaviors of AIE, TADF, RTP, dual-RTP and Mechanoluminescence from Simple Organic Molecules by Positional Isomerism

Yu Xiong, Junyi Gong, Junkai Liu, Deliang Wang, Hongzhuo Wu, Zheng Zhao, Manman Fang, Zhen Li, Dong Wang* and Ben Zhong Tang**

Table of Contents

1. General methods: All the reactions were carried out under a nitrogen atmosphere. The starting materials methyl 2-iodobenzoate, and *o-, m-, p*-chloroanilines, and reagents of Cu powder, CuI were purchased from commercial suppliers and used directly without further purification. ^{1}H NMR spectra were recorded on a Varian Mercury 400 NMR spectrometer in $CDCl_3$ using *tetra*-methylsilane as the internal standard. ^{13}C NMR spectra were recorded on the Bruker AVANCE III HD 600 MHz NMR spectrometer in $CDCl_3$ using *tetra*-methylsilane as the internal standard. High-resolution mass spectra were recorded on a Finnigan MAT TSQ7000 mass spectrometer system operated in a MALDI-TOF mode. High-performance

liquid chromatography (HPLC) was performed on the Waters e2695 HPLC system using an XBridge^{TM}-C18 column (5 mm). The running buffer was 30%H_2O-70%MeOH. The UV-*vis* absorption spectra were recorded on a UV-2600 spectrophotometer, and the photoluminescence spectra were recorded on a PerkinElmer LS 55 fluorescence spectrometer. Absolute quantum yields were measured by integrating sphere on a Horiba Fluorolog-3 spectrofluorometer. The lifetimes were measured on an Edinburgh FLS980 fluorescence spectrophotometer equipped with a continuous xenon lamp (Xe1), a microsecond pulsed xenon flashlamp (uF920), and a nanosecond flashlamp lamp (nF920), respectively. Single crystal data were collected on a Bruker Smart APEXII CCD diffractometer using graphite monochromated Mo Kα radiation (λ = 0.71073 Å) or Cu Kα radiation (λ = 1.54184 Å). Elemental analysis was performed on an EL cube. The thermogravimetric analysis (TGA) measurements were performed on a TA Instrument TGA Q5000. The differential scanning calorimetry (DSC) measurements were performed on a TA Instrument DSC Q1000. The photos and videos were recorded by a Canon EOS 70D and mobile phone Huawei Pro30.

2. Synthesis of target compounds

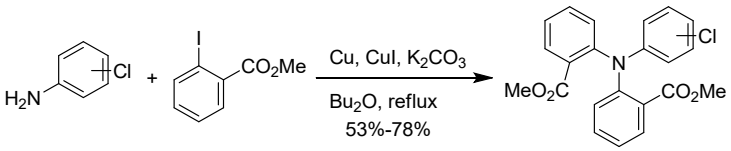

Scheme S1. Synthetic route of isomers *o*-ClTPA, *m*-ClTPA, and *p*-ClTPA.

General experimental procedure: A three-neck flask equipped with a reflux condensing tube was charged with methyl 2-iodobenzoate (3.93 g, 15.0 mmol), chloroaniline (0.64 g, 5.0 mmol), K_2CO_3 (1.80 g, 13.0 mmol), Cu (63.6 mg, 1.0 mmol), and CuI (95.2 mg, 0.25 mmol) under nitrogen atmosphere. *n*-butyl ether was injected into the flask and the resulting mixture was heated to reflux under stirring for 48 h. After cooling to room temperature, the solvent was removed under reduced pressure, and the resulting residue was dissolved in dichloromethane and filtered through celite. The collected filtrate was concentrated under reduced pressure and the crude product was purified by silica-gel column chromatography using dichloromethane/hexane as the eluent, followed by recrystallization two times from dichloromethane/hexane to yield crystal.

Compound *o*-ClTPA: Yield: 1.11 g, 56%. ^{1}H NMR (400 MHz, $CDCl_3$) δ (ppm): 7.66 (dd, J_1 = 8.0 Hz, J_2 = 7.6 Hz, 1H), 7.59 (dd, J_1 = 1.2 Hz, J_2 = 7.6 Hz, 1H), 7.40–7.32(m, 3H), 7.17–6.95 (m, 7H), 3.43 (s, 3H), 3.40 (s, 3H). ^{13}C NMR (150 MHz, $CDCl_3$) δ (ppm): 167.9, 167.8, 146.7, 146.6, 144.7, 132.3, 132.1, 131.2, 131.2, 130.9, 130.1, 128.4, 127.5, 127.3, 126.9, 125.9, 125.7, 125.5, 123.8, 123.1, 51.8, 51.6. HR-MS (MALDI-TOF), *m*/*z*: calcd for $C_{22}H_{18}ClNO_4$, 395.0924.

Found, 395.0941. Elemental analysis calcd for $C_{22}H_{18}ClNO_4$: C, 66.75; H, 4.58; N, 3.54. Found: C, 66.50; H, 4.46; N, 3.35.

Compound *m*-ClTPA: Yield: 1.05 g, 53%. ^{1}H NMR (400 MHz, $CDCl_3$) δ (ppm): 7.71–7.69 (m, 2H), 7.46–7.42 (m, 2H), 7.22–7.18 (m, 4H), 7.04 (t, J = 8.0 Hz,1H), 6.82 (dt, J_1 = 0.8 Hz, J_2 = 8.0 Hz, 1H), 6.69 (t, J = 2.0 Hz,1H), 6.60 (dd, J_1 = 2.0 Hz, J_2 = 8.0 Hz, 1H), 3.46 (s, 6H). ^{13}C NMR (150 MHz, $CDCl_3$) δ (ppm): 167.4, 149.7, 145.6, 134.6, 132.9, 131.1, 129.9, 129.2, 129.1, 128.1, 124.8, 121.2, 119.8, 118.0, 51.9. HR-MS (MALDI-TOF), *m*/*z*: calcd for $C_{22}H_{18}ClNO_4$, 395.0924. Found, 395.0968. Elemental analysis calcd for $C_{22}H_{18}ClNO_4$: C, 66.75; H, 4.58; N, 3.54. Found: C, 66.40; H, 4.41; N, 3.41.

Compound *p*-ClTPA: Yield: 1.54 g, 78%. ^{1}H NMR (400 MHz, $CDCl_3$) δ (ppm): 7.69–7.67 (m, 2H), 7.45–7.41 (m, 2H), 7.20–7.16 (m, 4H), 7.08 (d, J = 8.8 Hz, 2H), 6.67 (d, J = 8.8 Hz, 2H), 3.45 (s, 6H). ^{13}C NMR (150 MHz, $CDCl_3$) δ (ppm): 167.5, 147.3, 146.0, 132.9, 131.1, 128.9, 128.9, 127.9, 126.2, 124.5, 121.3, 51.9. HR-MS (MALDI-TOF), *m*/*z*: calcd for $C_{22}H_{18}ClNO_4$, 395.0924. Found, 395.0912. Elemental analysis calcd for $C_{22}H_{18}ClNO_4$: C, 66.75; H, 4.58; N, 3.54. Found: C, 66.45; H, 4.29; N, 3.42.

3. Computational methods: The quantum mechanics/molecular mechanics (QM/MM) method was implemented to optimize the geometries and calculate the electronic structures of the three compounds in crystal by virtue of ChemShell 3.5,[1] interfacing Turbomole 6.5[2] for QM and DL_POLY[3] with the general Amber force field (GAFF)[4] for MM. The computational models were built by digging a 5×5×5 supercell from the X-ray crystal structure, and the central molecule acts as the QM part and the surrounding molecules are treated as MM part, as shown in Chart S1-S3. The geometries of QM molecules were fully optimized at B3LYP/6-31G(d) level and the surrounding MM ones were frozen for the three molecular cluster models. The atomic partial charges were generated by the restrained electrostatic potential (RESP) method.[5] Based on the optimized geometries in the ground state (S_0), the excitation energies were calculated by using TD/B3LYP/6-31G(d) for the electronic excited singlet and triplet states. At the same level, the spin-orbit coupling (SOC) matrix elements between singlet and triplet states are given by Beijing Density Function (BDF) program.[6-8]

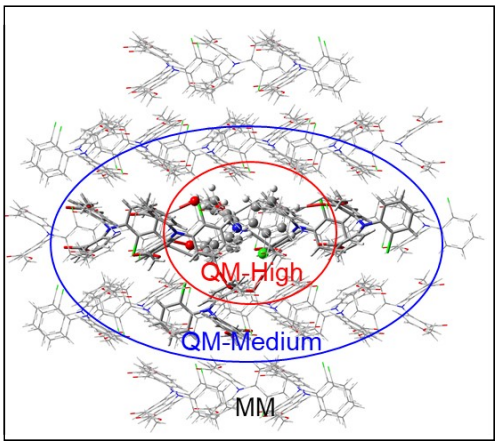

Chart S1. QM/MM model of isomer *o*-ClTPA: one central QM molecule for the higher layer and the surrounding MM molecules for the lower layer.

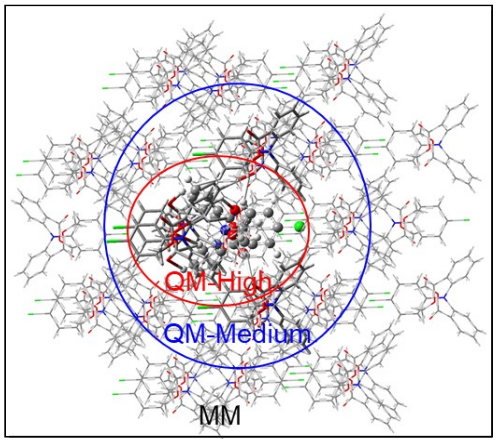

Chart S2. QM/MM model of isomer *m*-ClTPA: one central QM molecule for the higher layer and the surrounding MM molecules for the lower layer.

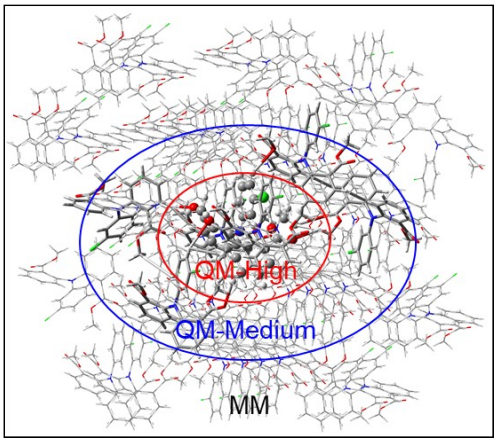

Chart S3. QM/MM model of isomer *p*-ClTPA: one central QM molecule for the higher layer and the surrounding MM molecules for the lower layer.

4. Supporting Figures and Tables

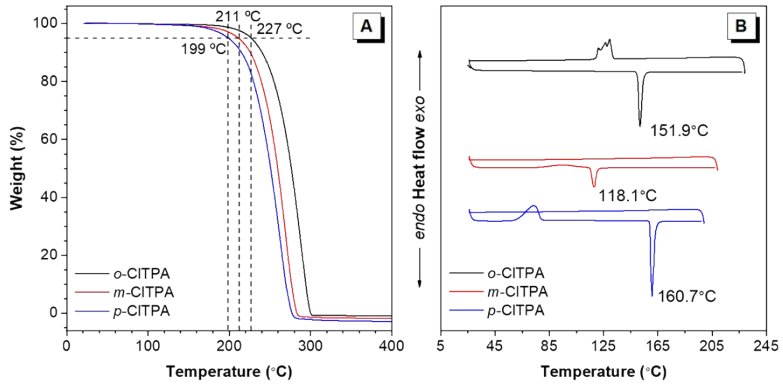

Figure S1. (A-B) TGA thermograms and DSC curves of isomers *o*-ClTPA, *m*-ClTPA, and *p*-ClTPA recorded under nitrogen at a heating rate of 10°C/min.

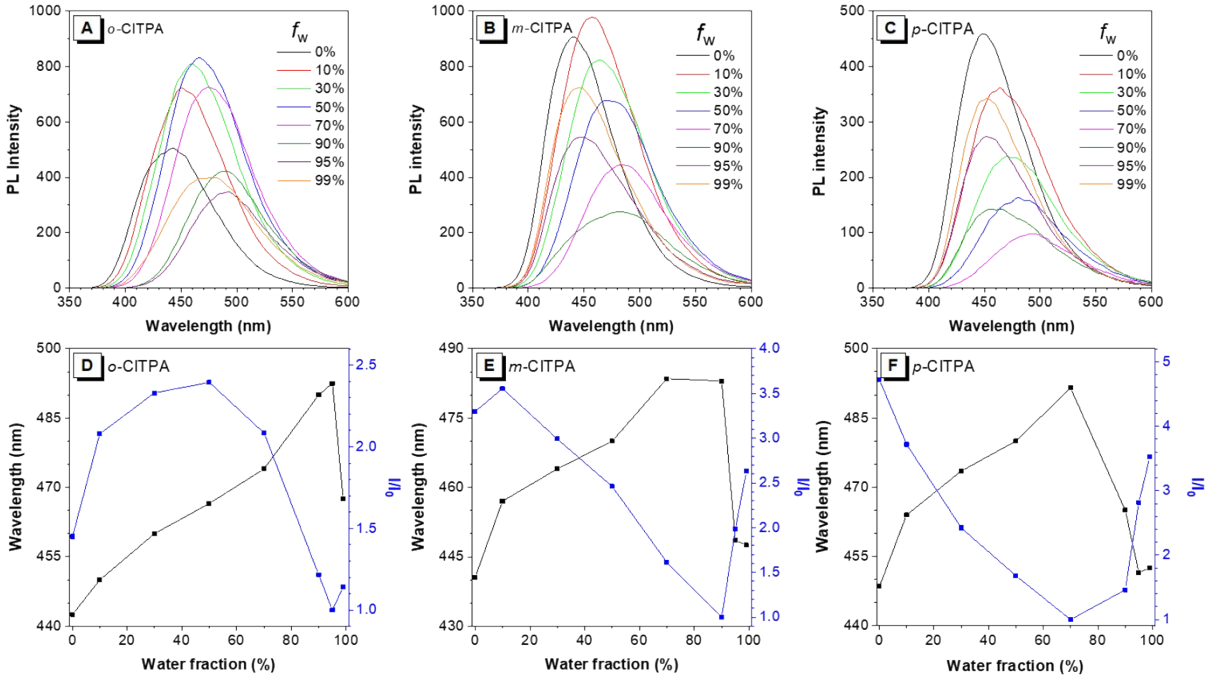

Figure S2. (A-C) Steady-state PL spectra of isomers *o*-ClTPA, *m*-ClTPA, and *p*-ClTPA in THF/water mixtures with different water fractions (f_w); (D-F) change in PL maximum and relative PL intensity (I/I_0) of isomers *o*-ClTPA, *m*-ClTPA, and *p*-ClTPA in THF/water mixtures with different water fractions. I_0 = PL intensity at f_w = 95%, 90% and 70%, respectively. Concentration: 10 μM; excitation wavelength: 300 nm.

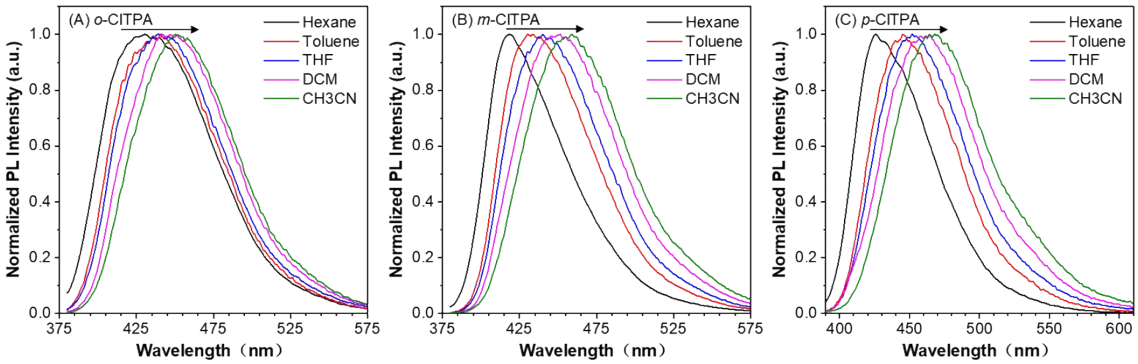

Figure S3. (A-C) Steady-state PL spectra of isomers *o*-ClTPA, *m*-ClTPA, and *p*-ClTPA in select solvents with increasing polarity. Concentration: 10 μM; excitation wavelength: 300 nm.

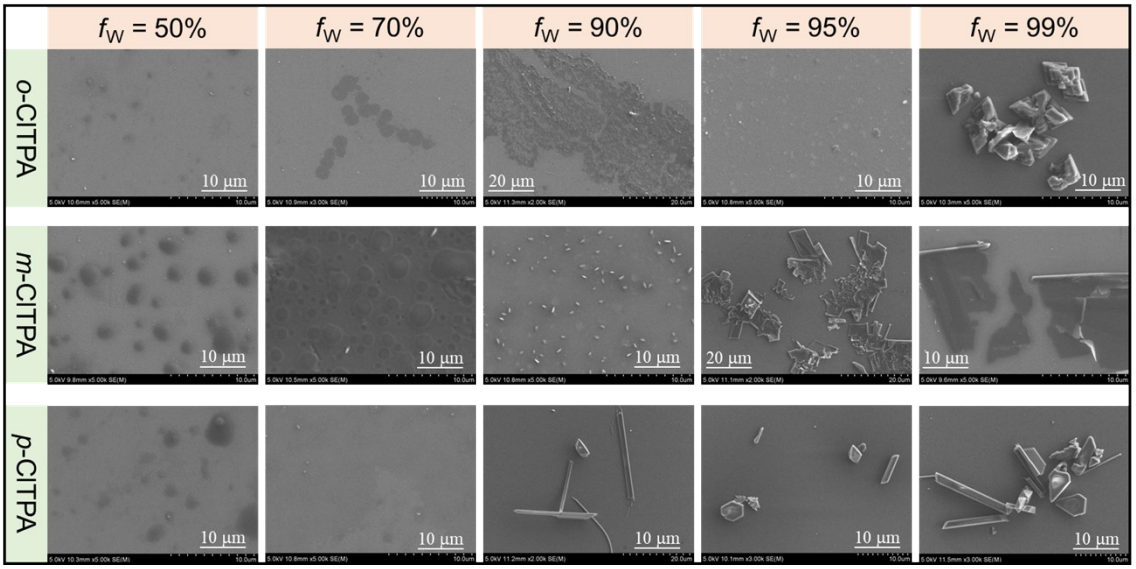

Figure S4. SEM images of isomers *o*-ClTPA, *m*-ClTPA, and *p*-ClTPA in THF/water mixtures with different water fractions (f_w).

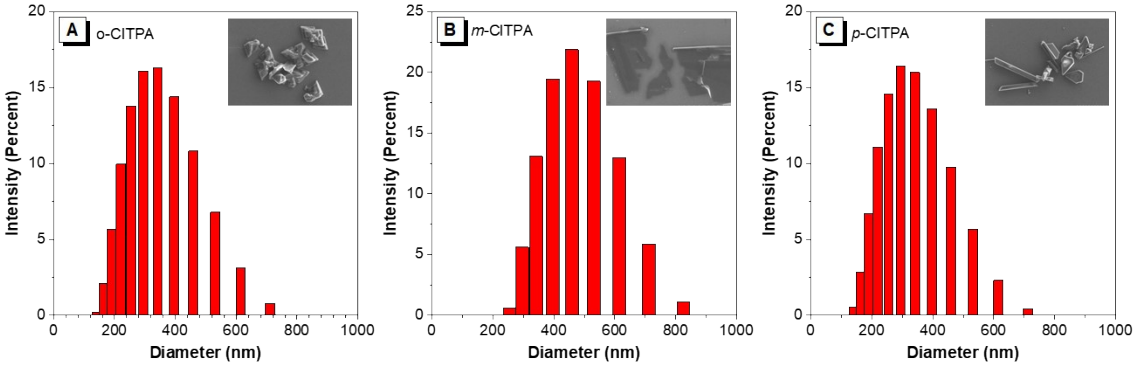

Figure S5. (A-C) Dynamic light scattering (DLS) result shows the diameter of isomers *o*-ClTPA, *m*-ClTPA, and *p*-ClTPA in THF/water mixtures with 99% water fractions (Concentration: 10 μM). Inset is an SEM image of corresponding nanoparticles.

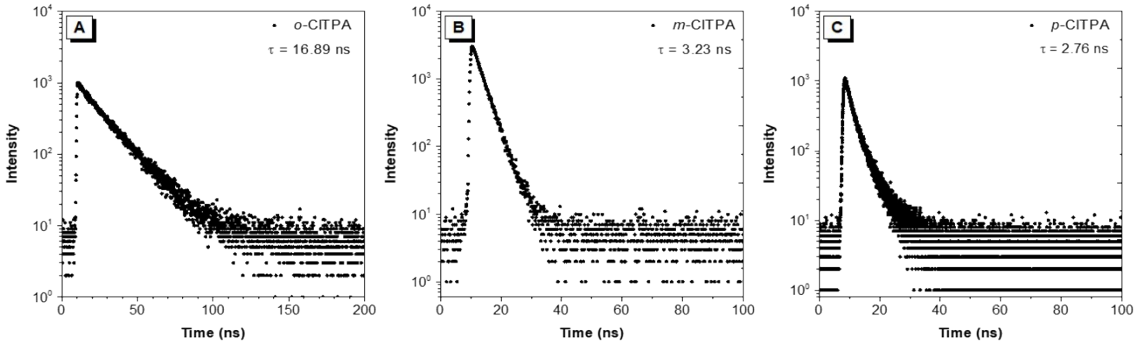

Figure S6. Transient prompt emission decay curves of isomers *o*-ClTPA, *m*-ClTPA, and *p*-ClTPA in crystalline solid at room temperature.

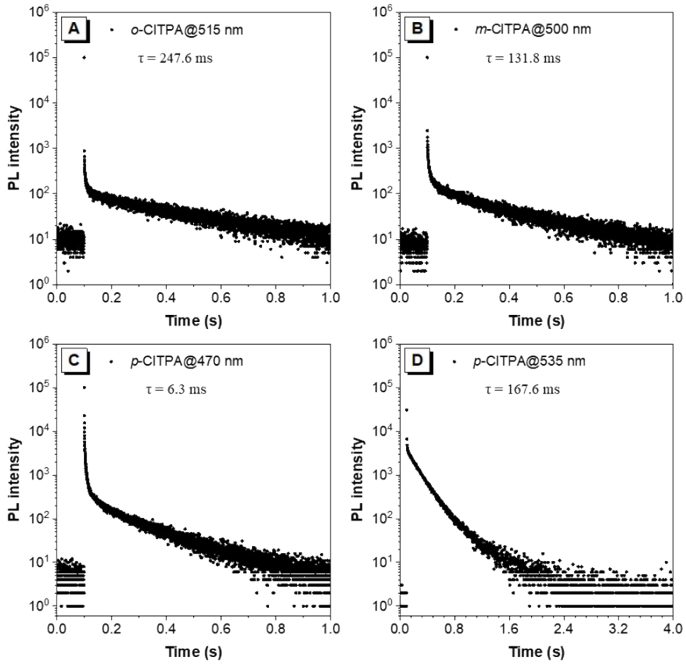

Figure S7. (A-D) Transient delayed emission decay curves of isomers o-ClTPA, m-ClTPA, and p-ClTPA in crystalline solid at 77 K.

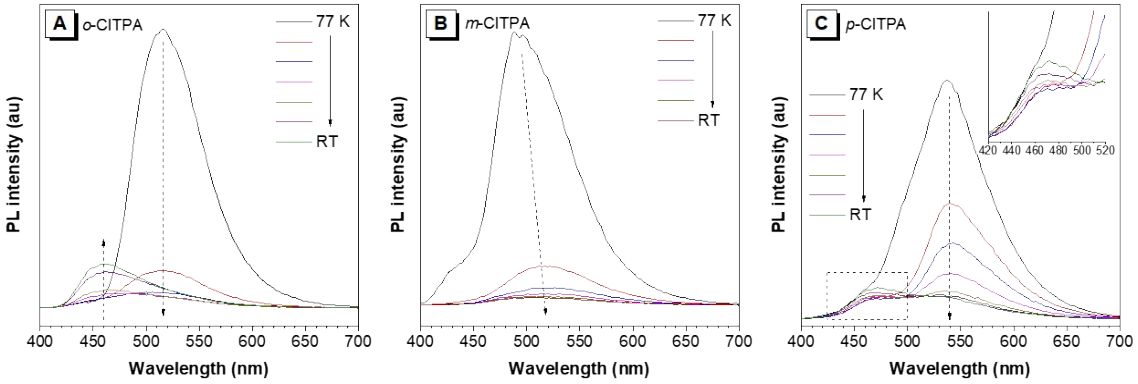

Figure S8. (A-C) Temperature-dependent delayed PL spectra of isomers *o*-ClTPA, *m*-ClTPA, and *p*-ClTPA in crystalline solid.

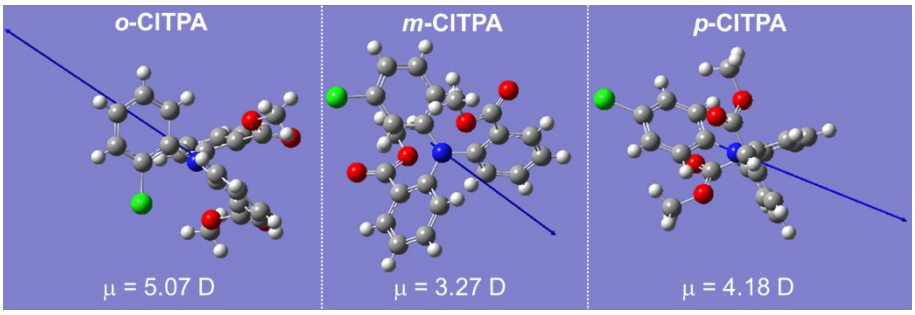

Figure S9. Calculated dipole moments of isomers *o*-ClTPA, *m*-ClTPA, and *p*-ClTPA in the crystal state.

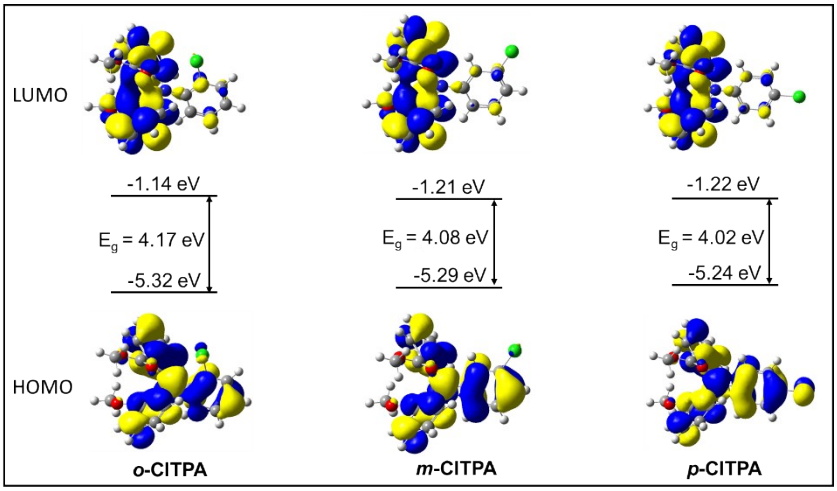

Figure S10. Calculated frontier molecular orbitals including HOMO and LUMO of isomers *o*-ClTPA, *m*-ClTPA, and *p*-ClTPA in the gas phase.

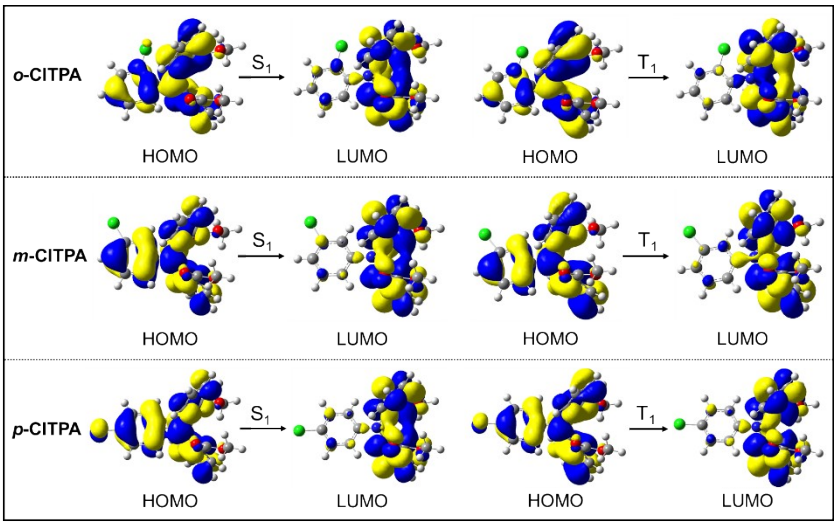

Figure S11. The NTOs of isomers *o*-ClTPA, *m*-ClTPA, and *p*-ClTPA calculated in the gas phase.

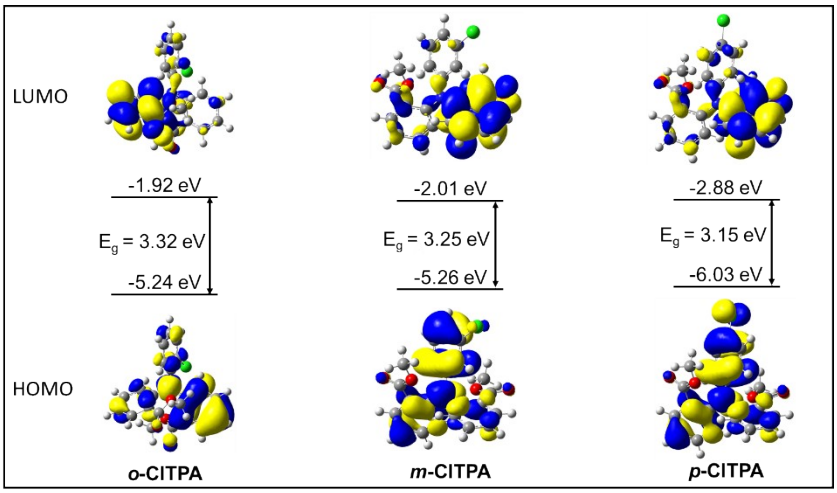

Figure S12. Calculated frontier molecular orbitals including HOMO and LUMO of isomers *o*-ClTPA, *m*-ClTPA, and *p*-ClTPA in the crystal phase.

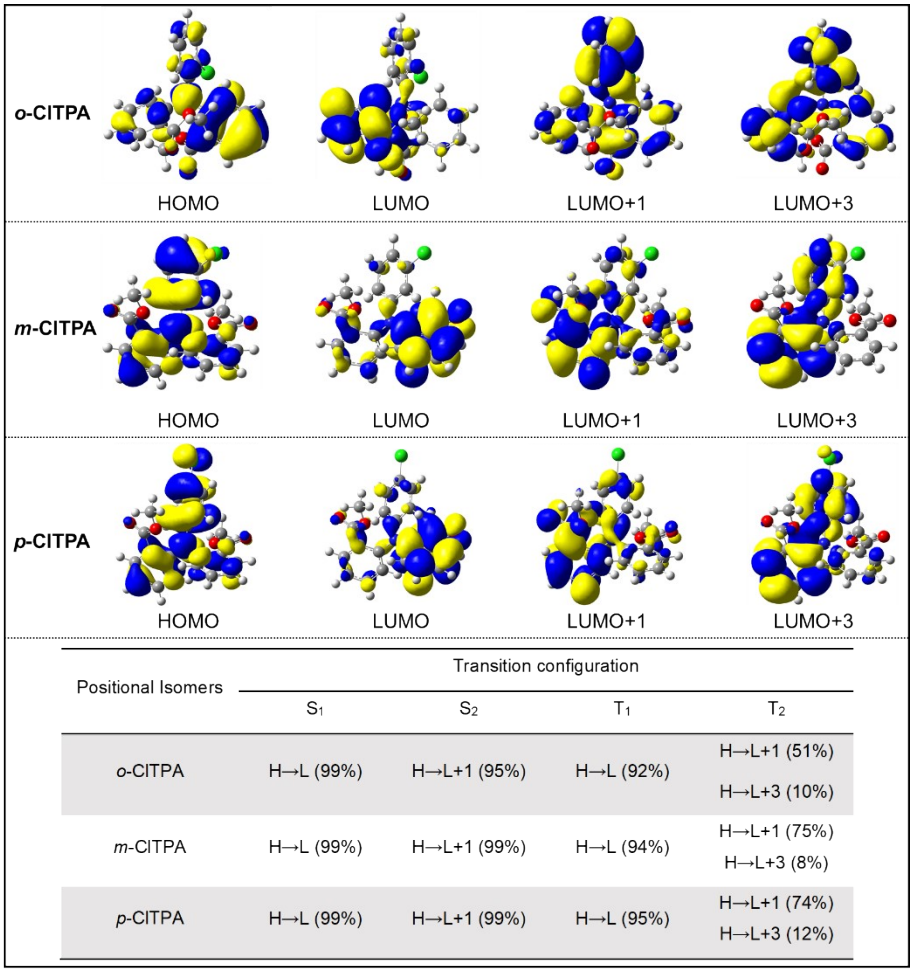

Positional Isomers	Transition configuration			
	S_1	S_2	T_1	T_2
o-ClTPA	H→L (99%)	H→L+1 (95%)	H→L (92%)	H→L+1 (51%) H→L+3 (10%)
m-ClTPA	H→L (99%)	H→L+1 (99%)	H→L (94%)	H→L+1 (75%) H→L+3 (8%)
p-ClTPA	H→L (99%)	H→L+1 (99%)	H→L (95%)	H→L+1 (74%) H→L+3 (12%)

Figure S13. The HOMO and LUMO distributions, and transition configurations of excited states of isomers *o*-ClTPA, *m*-ClTPA, and *p*-ClTPA calculated in the crystal phase.

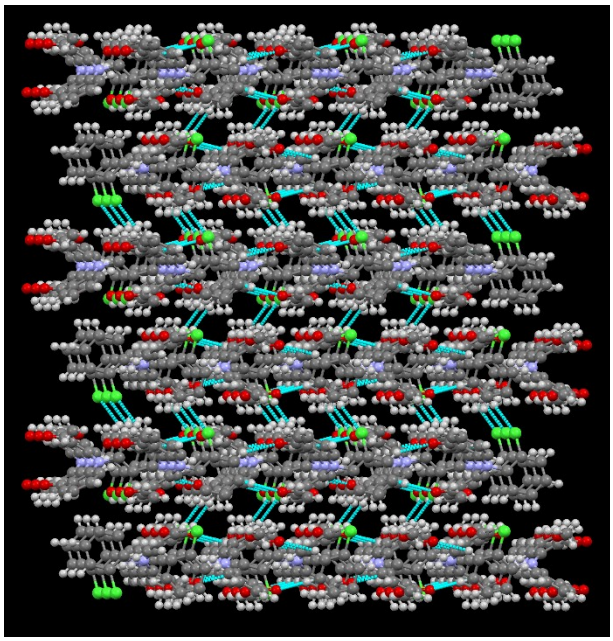

Figure S14. Packing mode of isomer *o*-ClTPA in crystal.

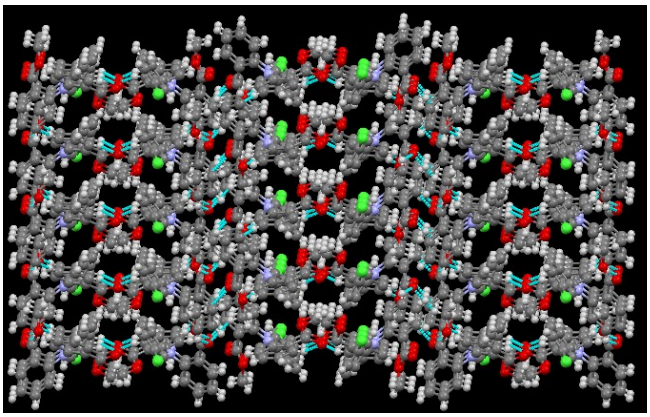

Figure S15. Packing mode of isomer *m*-ClTPA in crystal.

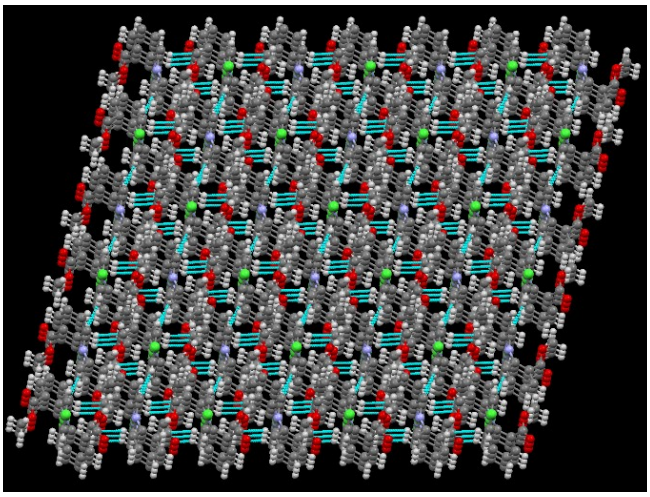

Figure S16. Packing mode of isomer *p*-ClTPA in crystal.

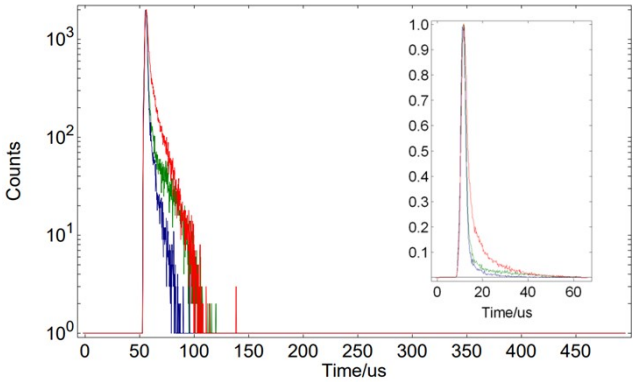

Figure S17. The temporal output of uF920H Xenon Flashlamp of FLS 980 measured at 300nm (blue), 450nm (green), and 600nm (red). The typical pulse width is 2μs.

Table S1. Single crystal data of isomers *o*-ClTPA, *m*-ClTPA and *p*-ClTPA.

Isomer	*o*-ClTPA	*m*-ClTPA	*p*-ClTPA
Crystal system	monoclinic	monoclinic	monoclinic
Space group	$P2_1/n$ (centrosymmetry)	C2/c (centrosymmetry)	I2/a (C2/c) (centrosymmetry)
a/Å	10.6439(2)	12.3359(8)	12.3515(2)
b/Å	13.6702(3)	10.0026(10)	13.5365(2)
c/Å	13.2289(3)	31.219(3)	11.8984(2)
α/°	90	90	90
β/°	92.649(2)	90.085(6)	104.6010(10)
γ/°	90	90	90
Volume/Å^3	1922.80(7)	3852.1(6)	1925.12(5)
Z	4	8	4
ρ_{calc}g/cm^3	1.367	1.365	1.366
μ/mm^{-1}	2.001	0.227	1.999
F(000)	824	1648	824
h, k, lmax	12, 16, 15	15, 12, 39	14, 15, 13
Nref	3236	4053	1628
Tmin,Tmax	0.866, 1.000	0.451, 1.000	0.808, 1.000
R(reflections)	0.0803(2860)	0.0683(3243)	0.0302(1548)
wR2(reflections)	0.2263(3236)	0.1772(4053)	0.0824(1628)
Data completeness	0.992	0.965	0.992
Theta(max)	64.995	26.988	64.962
S	1.032	1.091	1.101
Npar	255	255	130

a) The single-crystal structures have been deposited at the Cambridge Crystallographic Data Centre and allocated the deposition number: *o*-ClTPA (1816586), *m*-ClTPA (1816585), and *p*-ClTPA (1816587).

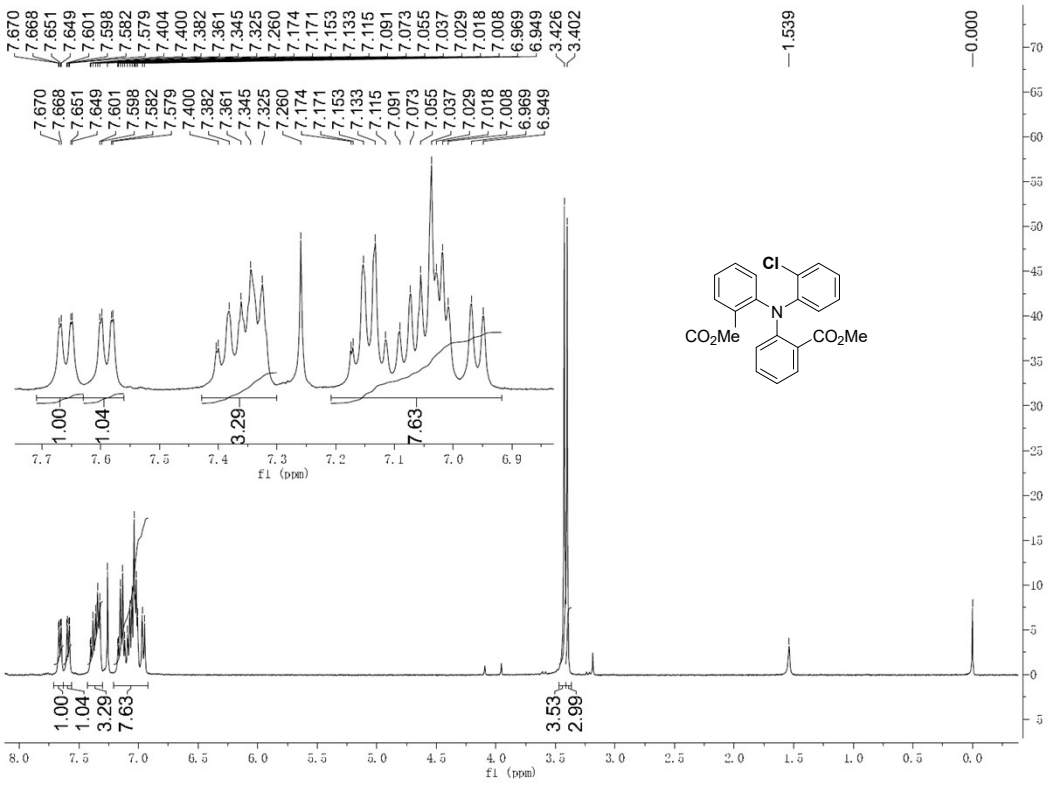

Figure S18. ^{1}H NMR spectrum of compound *o*-ClTPA in $CDCl_3$.

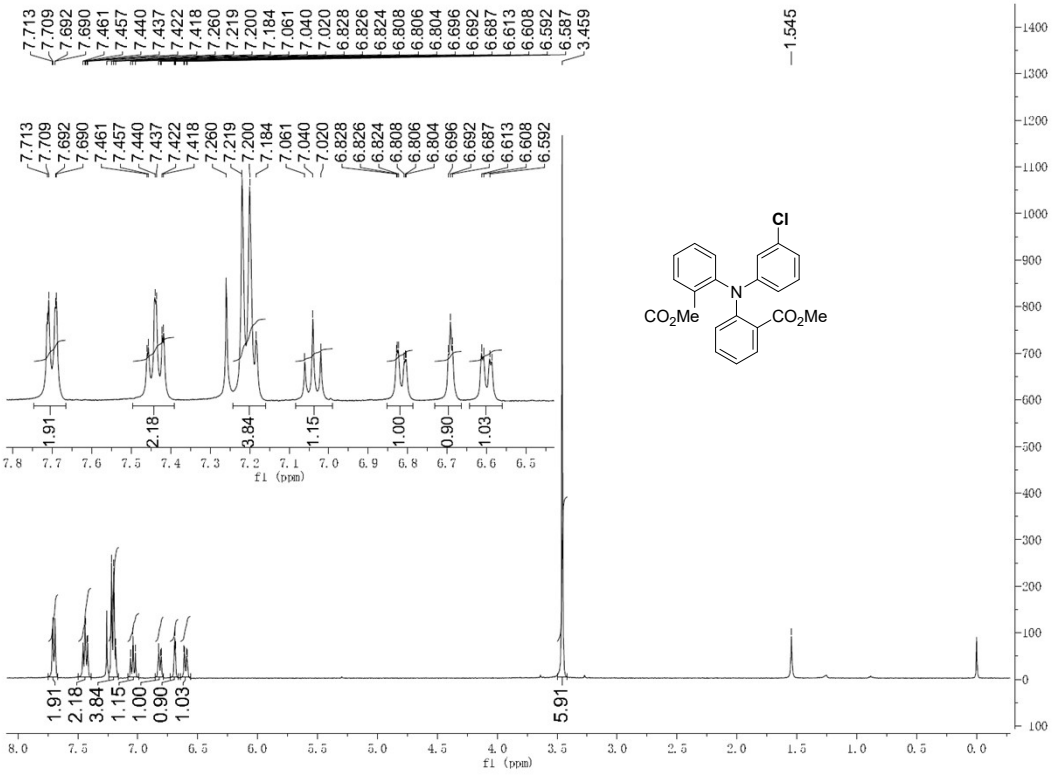

Figure S19. ^{1}H NMR spectrum of compound *m*-ClTPA in $CDCl_3$.

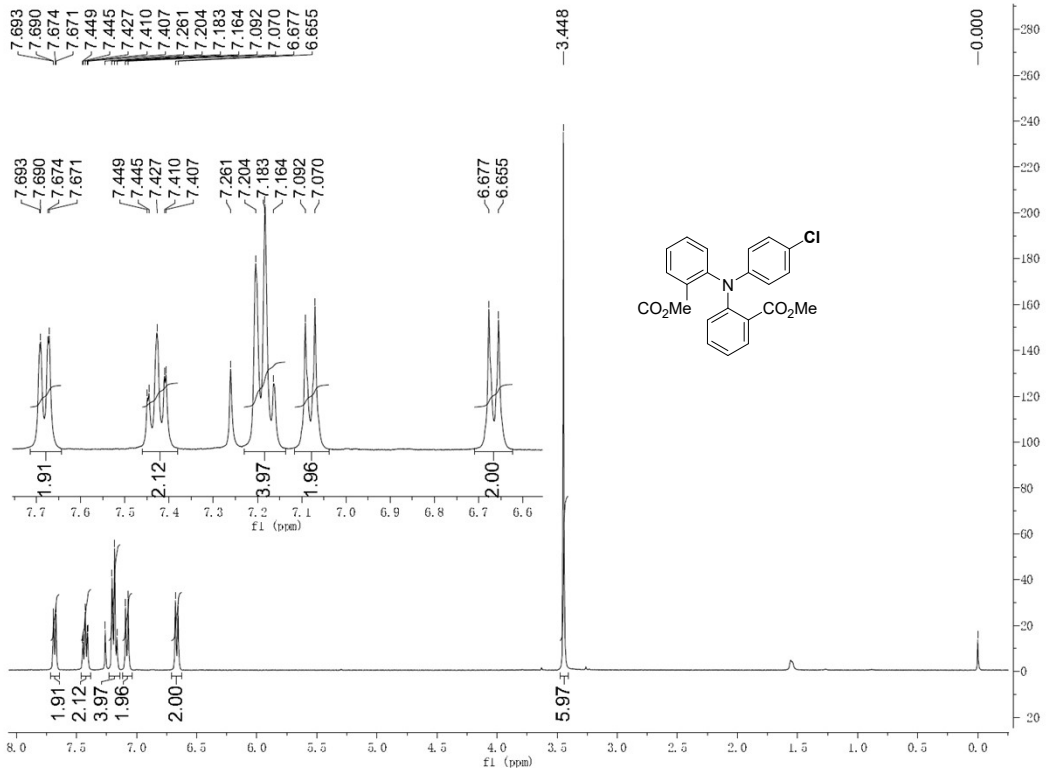

Figure S20. ^{1}H NMR spectrum of compound *p*-ClTPA in $CDCl_3$.

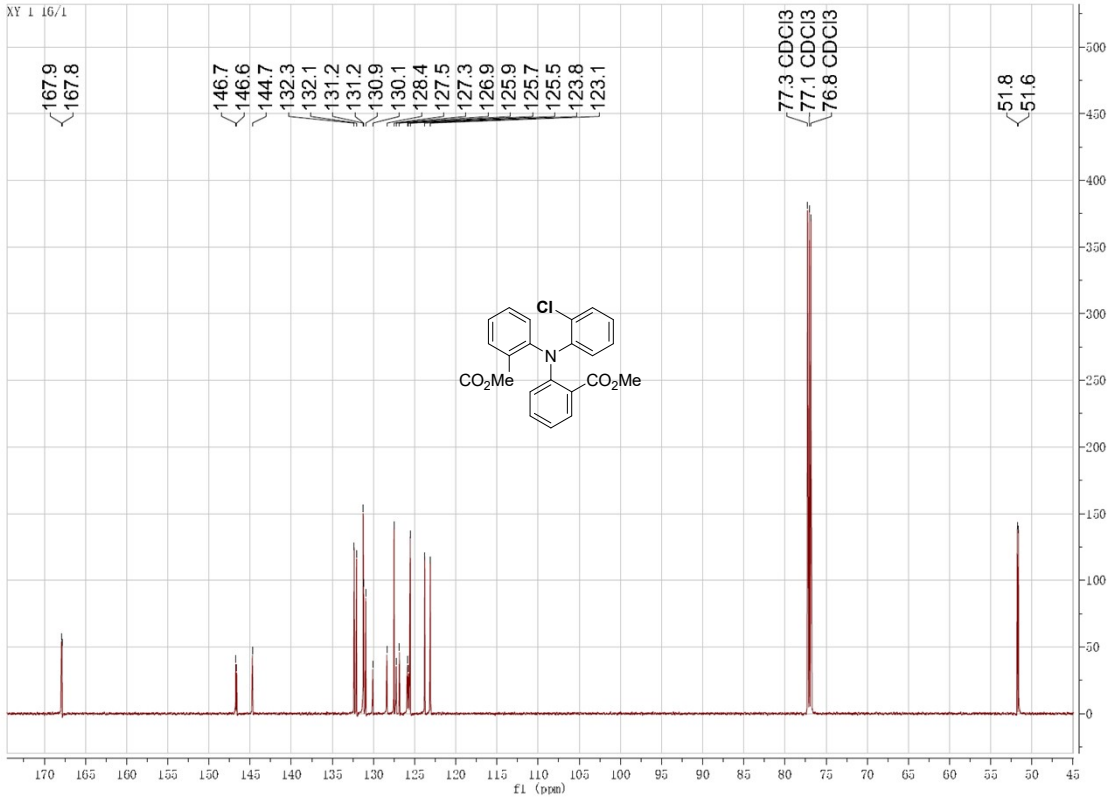

Figure S21. ^{13}C NMR spectrum of compound *o*-ClTPA in $CDCl_3$.

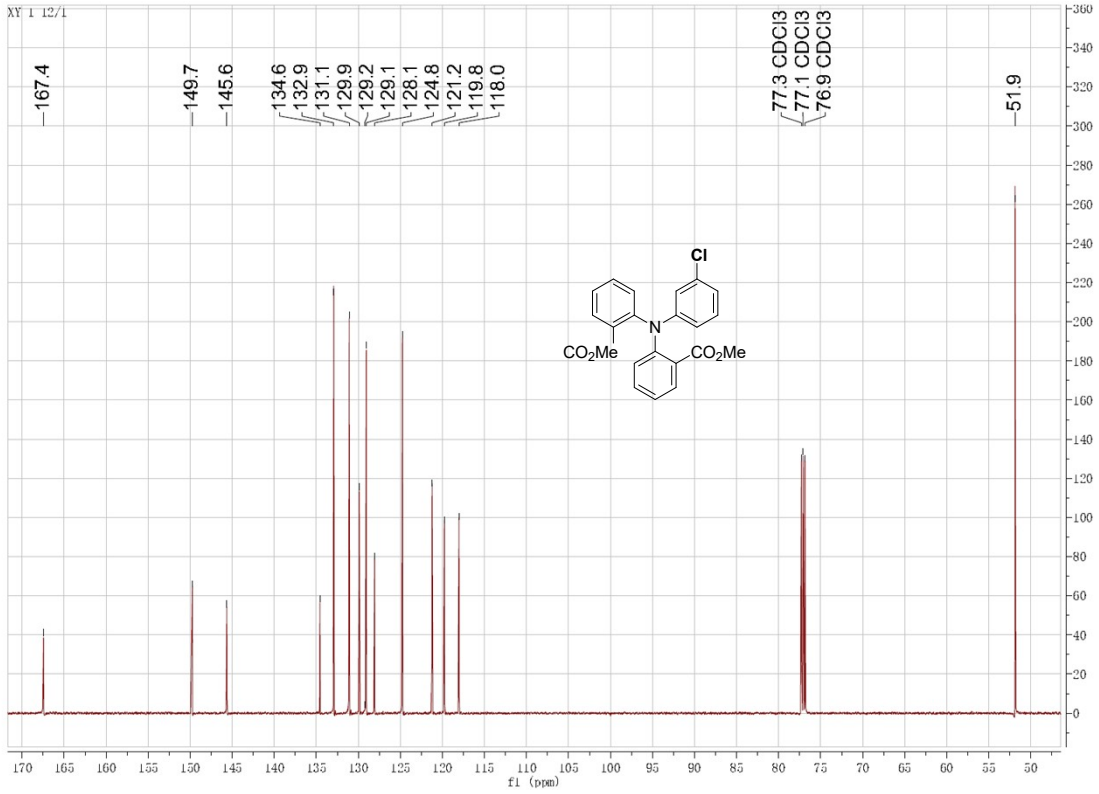

Figure S22. ^{13}C NMR spectrum of compound *m*-ClTPA in $CDCl_3$.

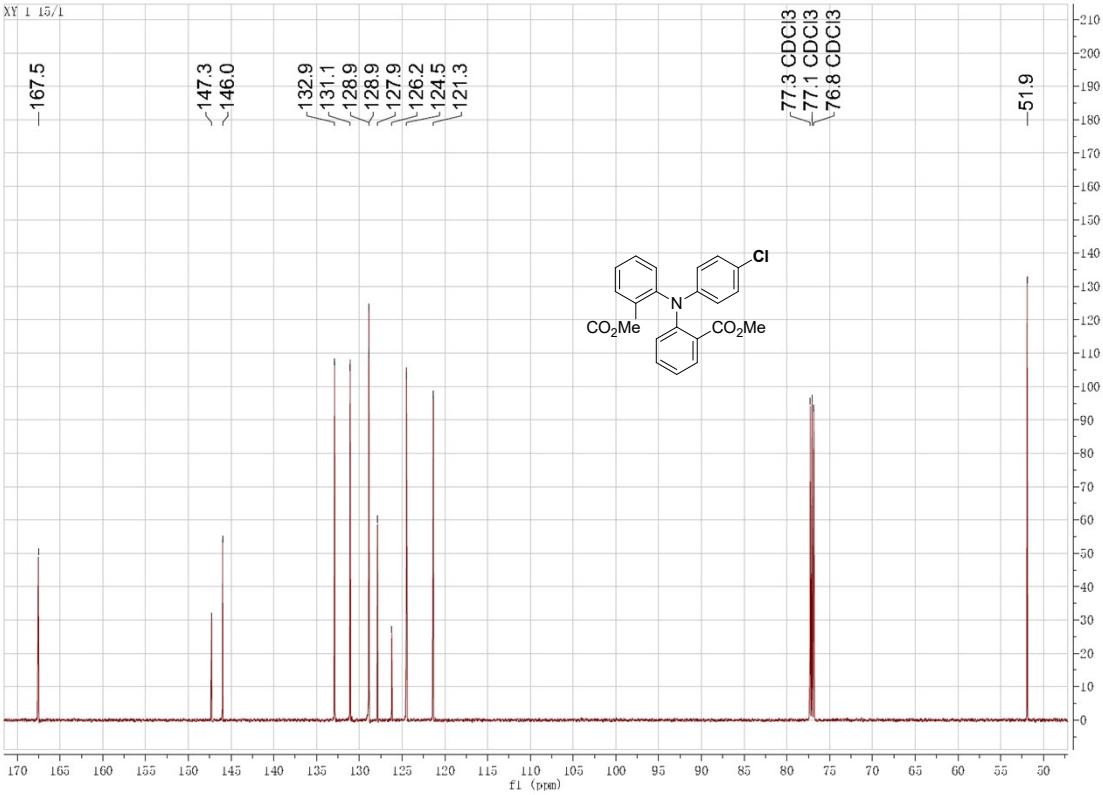

Figure S23. ^{13}C NMR spectrum of compound *p*-ClTPA in $CDCl_3$.

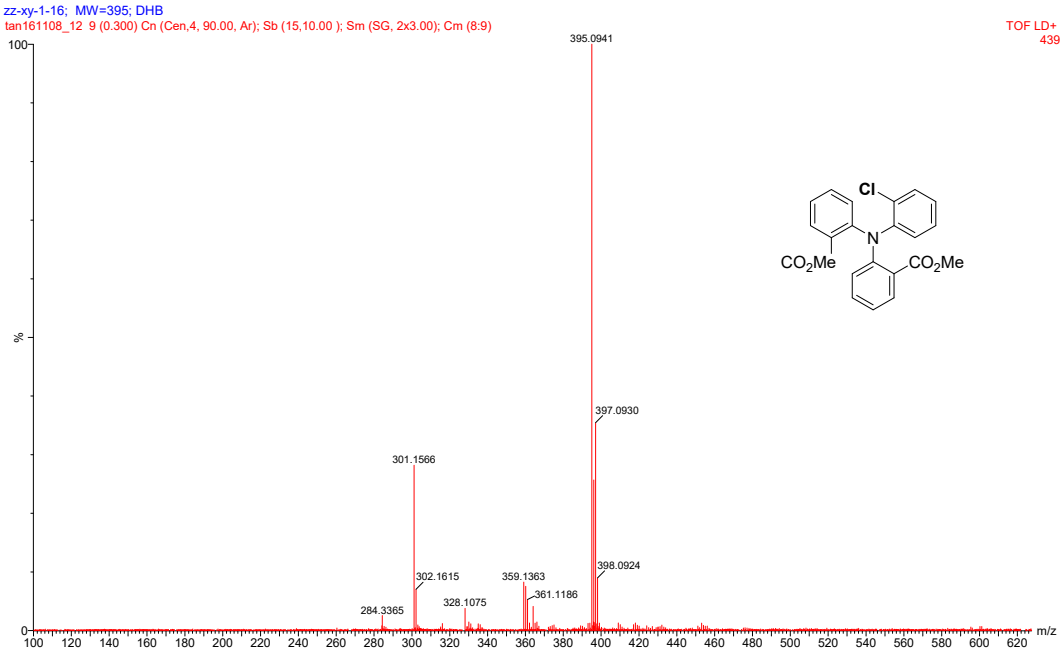

Figure S24. MALDI-TOF mass spectrum of compound *o*-ClTPA.

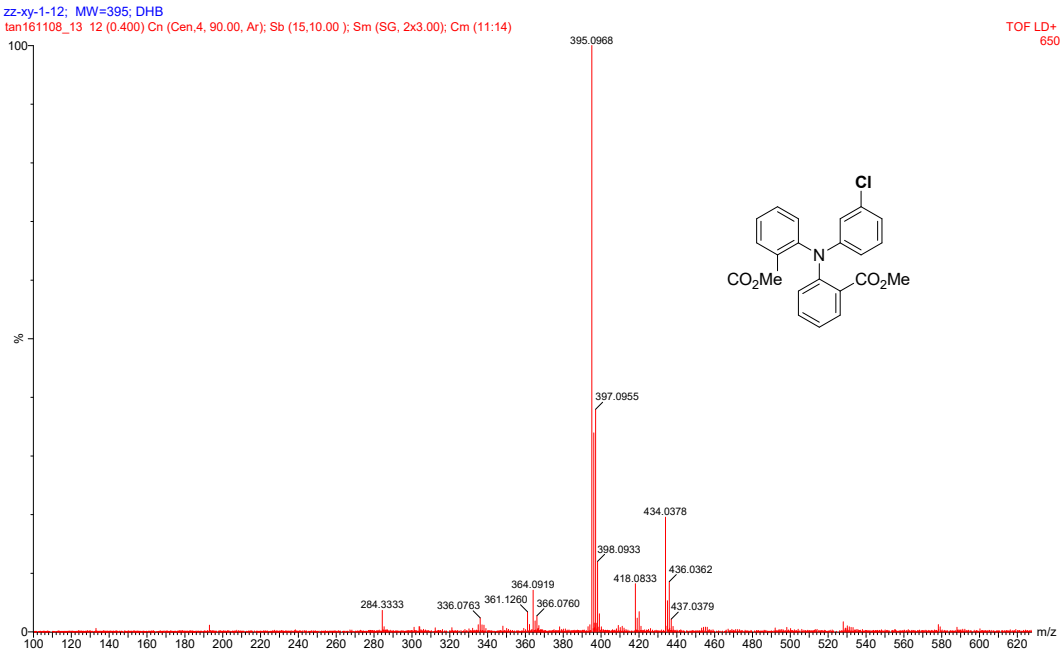

Figure S25. MALDI-TOF mass spectrum of compound *m*-ClTPA.

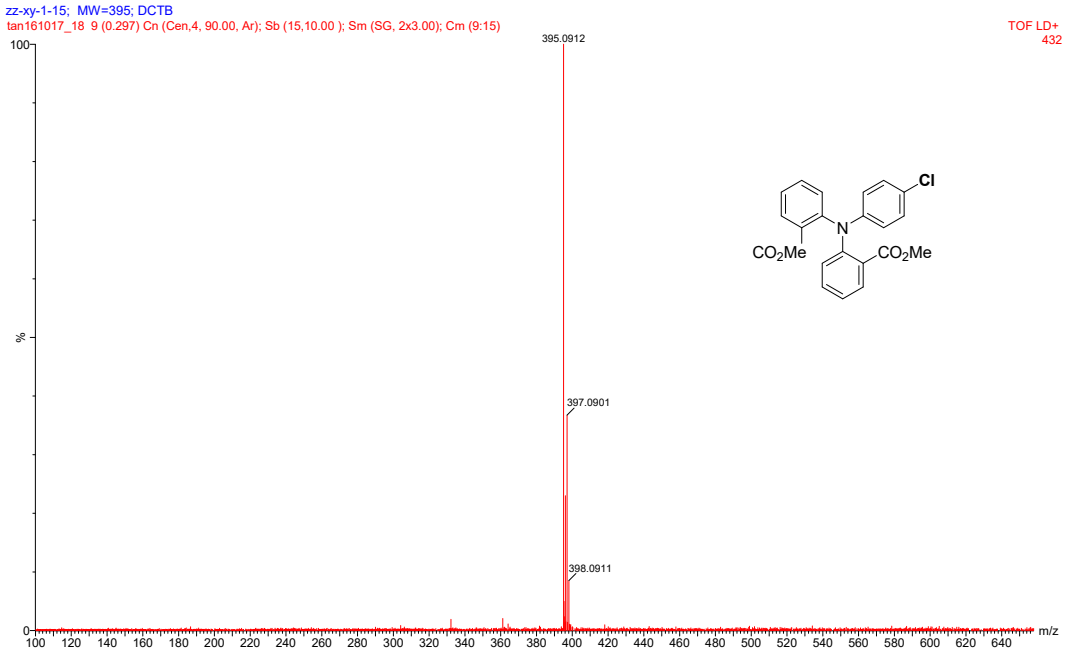

Figure S26. MALDI-TOF mass spectrum of compound *p*-ClTPA.

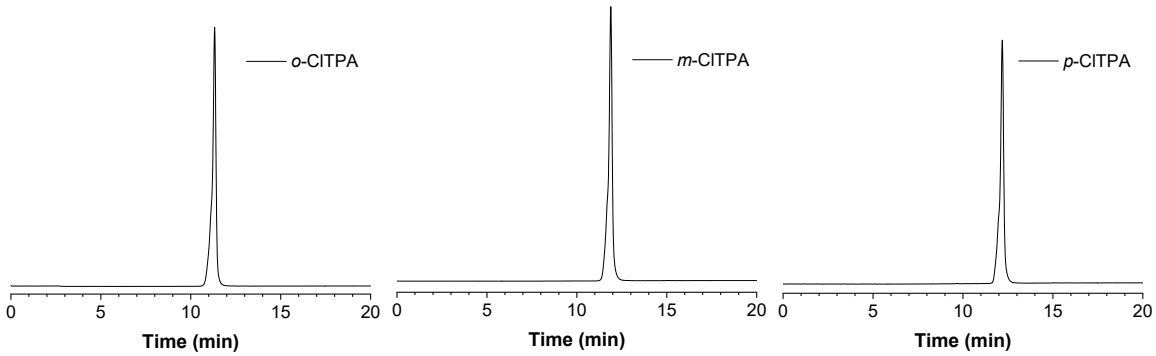

Figure S27. High-performance liquid chromatography diagrams of isomers *o*-ClTPA, *m*-ClTPA, and *p*-ClTPA.

5. References

[1] Sherwood, P.; de Vries, A. H.; Guest, M. F.; Schreckenbach, G.; Catlow, R. C. A.; French, S. A.; Sokol, A. A.; Bromley, S. T.; Thiel, W.; Turner, A. J.; Billeter, S.; Terstegen, F.; Thiel, S.; Kendrick, J.; Rogers, S. C.; Casci, J.; Watson, M.; King, F.; Karlsen, E.; Sjøvoll, M.; Fahmi, A.; Schäfer, A.; Lennartz, C. QUASI: A General Purpose Implementation of the QM/MM Approach and Its Application to Problems in Catalysis. *J. Mol. Struct.: Theochem.* **2003**, *632*, 1-28.

[2] Ahlrichs, R.; Bär, M.; Häser, M.; Horn, H.; Kölmel, C. Electronic Structure Calculations on Workstation Computers: The Program System Turbomole. *Chem. Phys. Lett.* **1989**, *162*, 165-169.

[3] Smith, W.; Forester, T. R. DL_POLY_2.0: A General-Purpose Parallel Molecular Dynamics Simulation Package. *J. Mol. Graph.* **1996**, *14*, 136-141.

[4] Wang, J.; Wolf, R. M.; Caldwell, J. W.; Kollman, P. A.; Case, D. A. Development and Testing of a General Amber Force Field. *J. Comput. Chem.* **2004**, *25*, 1157-1174.

[5] Bayly, C. I.; Cieplak, P.; Cornell, W.; Kollman, P. A. A Well-Behaved Electrostatic Potential Based Method Using Charge Restraints for Deriving Atomic Charges: The RESP Model. *J. Phys. Chem.* **1993**, *97*, 10269-10280.

[6] W. Liu, F. Wang, D. Dai, L. Li, M. Dolg, *Theor. Chem. Acc*. **1997**, *96*, 75-83.

[7] W. Liu, G. Hong, L. Li, *J. Theor. Comput. Chem*. **2003**, *2*, 257-272.

[8] K. Hirao, Y. Ishikawa, Recent Advances in Computational Chemistry, World Scientific, Singapore, **2004**, *5*, p257.